

Search for a pentaquark decaying to $\Xi^-\pi^-$

The FOCUS Collaboration¹

J. M. Link^a P. M. Yager^a J. C. Anjos^b I. Bediaga^b
 C. Castromonte^b A. A. Machado^b J. Magnin^b A. Massafferri^b
 J. M. de Miranda^b I. M. Pepe^b E. Polycarpo^b A. C. dos Reis^b
 S. Carrillo^c E. Casimiro^c E. Cuautle^c A. Sánchez-Hernández^c
 C. Uribe^c F. Vázquez^c L. Agostino^d L. Cinquini^d
 J. P. Cumalat^d V. Frisullo^d B. O'Reilly^d I. Segoni^d
 K. Stenson^d J. N. Butler^e H. W. K. Cheung^e G. Chiodini^e
 I. Gaines^e P. H. Garbincius^e L. A. Garren^e E. Gottschalk^e
 P. H. Kasper^e A. E. Kreymer^e R. Kutschke^e M. Wang^e
 L. Benussi^f S. Bianco^f F. L. Fabbri^f A. Zallo^f M. Reyes^g
 C. Cawlf^h D. Y. Kim^h A. Rahimi^h J. Wiss^h R. Gardnerⁱ
 A. Kryemadhiⁱ Y. S. Chung^j J. S. Kang^j B. R. Ko^j
 J. W. Kwak^j K. B. Lee^j K. Cho^k H. Park^k G. Alimonti^l
 S. Barberis^l M. Boschini^l A. Cerutti^l P. D'Angelo^l
 M. DiCorato^l P. Dini^l L. Edera^l S. Erba^l P. Inzani^l
 F. Leveraro^l S. Malvezzi^l D. Menasce^l M. Mezzadri^l
 L. Moroni^l D. Pedrini^l C. Pontoglio^l F. Prelz^l M. Rovere^l
 S. Sala^l T. F. Davenport III^m V. Arenaⁿ G. Bocaⁿ
 G. Bonomiⁿ G. Gianiniⁿ G. Liguoriⁿ D. Lopes Pegnaⁿ
 M. M. Merloⁿ D. Panteaⁿ S. P. Rattiⁿ C. Riccardiⁿ P. Vituloⁿ
 C. Göbel^o J. Otalora^o H. Hernandez^p A. M. Lopez^p
 H. Mendez^p A. Paris^p J. Quinones^p J. E. Ramirez^p Y. Zhang^p
 J. R. Wilson^q T. Handler^r R. Mitchell^r D. Engh^s M. Hosack^s
 W. E. Johns^s E. Luiggi^s M. Nehring^s P. D. Sheldon^s
 E. W. Vaandering^s M. Webster^s M. Sheaff^t

^aUniversity of California, Davis, CA 95616

^bCentro Brasileiro de Pesquisas Físicas, Rio de Janeiro, RJ, Brazil

^cCINVESTAV, 07000 México City, DF, Mexico

^dUniversity of Colorado, Boulder, CO 80309

^eFermi National Accelerator Laboratory, Batavia, IL 60510

^f*Laboratori Nazionali di Frascati dell'INFN, Frascati, Italy I-00044*

^g*University of Guanajuato, 37150 Leon, Guanajuato, Mexico*

^h*University of Illinois, Urbana-Champaign, IL 61801*

ⁱ*Indiana University, Bloomington, IN 47405*

^j*Korea University, Seoul, Korea 136-701*

^k*Kyungpook National University, Taegu, Korea 702-701*

^l*INFN and University of Milano, Milano, Italy*

^m*University of North Carolina, Asheville, NC 28804*

ⁿ*Dipartimento di Fisica Nucleare e Teorica and INFN, Pavia, Italy*

^o*Pontificia Universidade Católica, Rio de Janeiro, RJ, Brazil*

^p*University of Puerto Rico, Mayaguez, PR 00681*

^q*University of South Carolina, Columbia, SC 29208*

^r*University of Tennessee, Knoxville, TN 37996*

^s*Vanderbilt University, Nashville, TN 37235*

^t*University of Wisconsin, Madison, WI 53706*

Abstract

We present a search for a pentaquark decaying strongly to $\Xi^- \pi^-$ in γN collisions at a center-of-mass energy up to 25 GeV/ c^2 . Finding no evidence for such a state in the mass range of 1480 MeV/ c^2 to 2400 MeV/ c^2 , we set limits on the yield and on the cross section times branching ratio relative to $\Xi^*(1530)^0$.

Key words:

PACS: 14.80.-j 13.60.Le 13.60.Rj

1 Introduction

The existence of bound multiquark states like $Q\bar{Q}q\bar{q}$ and the H dihyperon were first proposed by Jaffe [1,2,3] in 1977. Then 20 years later Diakonov *et al.* [4] proposed the existence of four quarks and one antiquark confined in a low-mass anti-decuplet configuration. In their calculations Diakonov made several predictions of masses and widths of exotic baryonic states such as the mass of the lightest state Θ^+ (previously called Z^+) at about 1530 MeV/ c^2 . There were also predictions of decay modes: $\Theta^+ \rightarrow pK_s^0$, $\Theta^+ \rightarrow nK^+$ and $\Xi_5^{--} \rightarrow \Xi^- \pi^-$ ².

¹ See <http://www-focus.fnal.gov/authors.html> for additional author information.

² The Ξ_5^{--} is also known as the $\phi(1860)^{--}$.

On the experimental side, the year 2003 was the beginning of “pentaquark observations.” The Θ^+ at about the predicted mass was the first candidate as noted in the PDG2004 [5], but searches by higher statistics experiments yielded negative results as noted by R. Schumacher [6].

In the case of the doubly strange pentaquark Ξ_5^{--} the only positive evidence is from NA49 [7]. Negative results were obtained by every other search: HERA-B [8], ALEPH [9], WA89 [10], HERMES [11], BABAR [12], ZEUS [13], COMPASS [14], E690 [15], as well as preliminary results from CDF [16].

This letter describes a search for the $\Xi_5^{--} \rightarrow \Xi^- \pi^-$ pentaquark candidate³ in electromagnetic interactions and extends the search for the singly strange Θ^+ discussed in [17] to the doubly strange state considered here.

2 Event reconstruction and selection

The FOCUS experiment took data during the 1996–7 fixed-target run at Fermilab. A photon beam obtained from bremsstrahlung of 300 GeV electrons and positrons impinged on a set of BeO targets. The first element in the spectrometer was the silicon strip detector array: four triplets of silicon strip planes used for track finding and vertexing. Each triplet was comprised of three closely spaced parallel planes with the strip directions rotated to provide a means for correlating hits in the three planes of the triplet and thus track coordinates. For most of the run, two pairs of silicon strips were also interleaved with the target segments for more precise vertexing [18]. Charged particles were tracked and momentum analyzed as they passed through one or two dipole magnets and three to five sets of multiwire proportional chambers with four planes each (as shown in Fig. 1). Three multicell threshold Čerenkov counters, two electromagnetic calorimeters, and two muon detectors provided particle identification. A trigger which required, among other things, $\gtrsim 25$ GeV of hadronic energy passed 6 billion events for reconstruction.

The data used for this analysis come from a subset of FOCUS data which contain cascade candidates ($\Xi^- \rightarrow \Lambda^0 \pi^-$ and $\Omega^- \rightarrow \Lambda^0 K^-$). The cascade decays used in this analysis are those which occur downstream of the silicon detector and with the Λ^0 daughter being fully reconstructed through the decay $\Lambda^0 \rightarrow p \pi^-$. The Ξ^- candidate is a reconstructed silicon track with direction and position consistent with the intersection of a reconstructed Λ^0 and a multiwire chamber track. The Λ^0 invariant mass is required to be between $1.10 \text{ GeV}/c^2$ and $1.13 \text{ GeV}/c^2$. The higher momentum track is chosen to be the proton because the small phase space of the $\Lambda^0 \rightarrow p \pi^-$ constrains the

³ Charged conjugate states are implied unless explicitly stated otherwise.

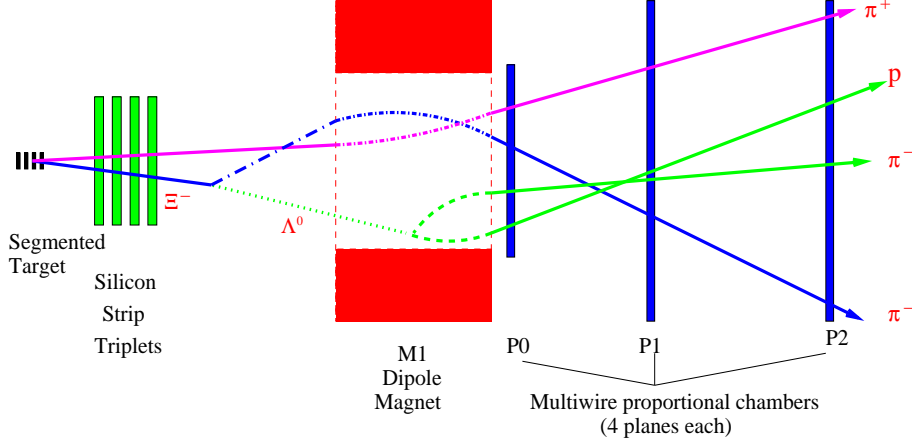


Fig. 1. A schematic drawing in the bend view of the spectrometer of a $\Xi^0(1530) \rightarrow \Xi^- \pi^+$ decay, with the Ξ^- decaying downstream the silicon strip detector, as described in the text. Only the front part of the spectrometer is displayed.

proton to carry most of the momentum for the decays observed in the forward FOCUS spectrometer. For this analysis we identify Ξ^- tracks when the matched Λ^0 candidate and the matched pion track have an invariant mass within $20 \text{ MeV}/c^2$ of the nominal Ξ^- signal peak (shadow region of fig. 2). The total sample yields approximately 625 000 $\Xi^- \rightarrow \Lambda^0 \pi^-$ signal events. A detailed description of the reconstruction of cascades and vees can be found in Ref. [19].

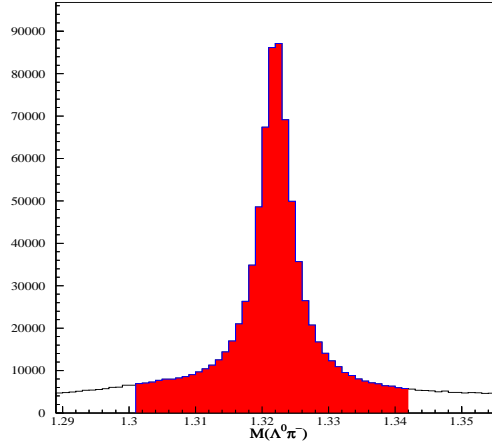


Fig. 2. The invariant mass plot represent the total sample of silicon tracks matched to a reconstructed Λ^0 and a multiwire chamber track (π^-). The shadow area is the region used to select Ξ^- tracks for this analysis.

Each Ξ^- track is combined with good quality charged tracks to make a vertex to search for $\Xi^*(1530)^0 \rightarrow \Xi^- \pi^+$ and $\Xi_5^- \rightarrow \Xi^- \pi^-$. This two track vertex must be well defined with a χ^2 probability greater than 1%. A multitrack production vertex is nucleated around this two track vertex and must be within 2σ of the $\Xi^- \pi$ vertex. The production vertex must have a χ^2 probability greater than 1% and must be within the target material or outside by no more than 3σ . In

both cases, σ is the calculated uncertainty on the vertex location or separation.

A particle identification algorithm has been developed which combines data from all of the Čerenkov counters which the track passes through. This algorithm [20] returns negative log-likelihood (times two) values W_i for a track and hypothesis $i \in \{e, \pi, K, p\}$ based on the light yields in the phototubes covering the Čerenkov cone of the track. A Čerenkov cut, $W_{\min(e,K,p)} - W_\pi > -8$, requires that the pion Ξ^- daughter (π^- track matched to Ξ^- track in Fig. 1) must not be strongly inconsistent with the pion hypothesis. For pions of the $\Xi^- \pi$ combination (π^+ track in Fig. 1) a Čerenkov cut, $W_{\min(e,K,p)} - W_\pi > -6$, is used to reduce combinatorial background.

Mass plots for $\Xi^- \pi^+$ are shown in Fig. 3 and in Fig. 4 with an additional cut that the $\Xi^- \pi^+$ momentum be greater than 25 GeV/c. The signal was best fit with a P-wave Breit-Wigner with an energy dependent width convoluted with a Gaussian for the detector resolution. The resolution, 2.92 MeV/c², was obtained from a Monte Carlo simulation and the fitted width of the Breit-Wigner is shown in the figures, consistent with the widths of 8-10 MeV/c² quoted in the PDG[5]. The background was fit to the form $aq^b \exp(cq + dq^2 + eq^3 + fq^4)$ where a — f are free parameters and q is the Q -value (invariant mass minus component masses).

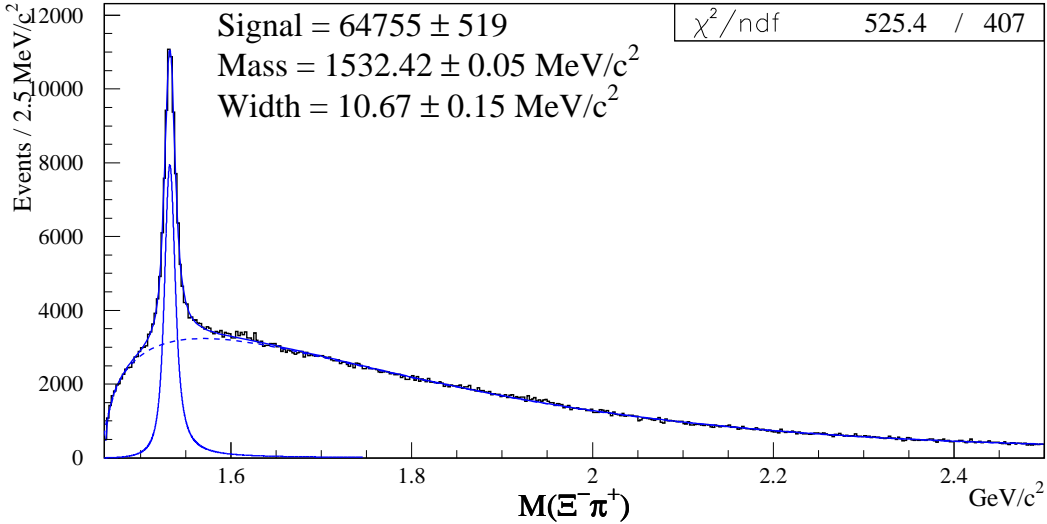


Fig. 3. $\Xi^*(1530)^0$ fit with a P-wave Breit-Wigner and combinatorial background.

3 Pentaquark search results

The $\Xi^- \pi^-$ and $\Xi^+ \pi^+$ invariant masses are plotted using the standard selection criteria in Fig. 5. There are no significant differences between the two charge states so for the remainder of the analysis we combine the charge con-

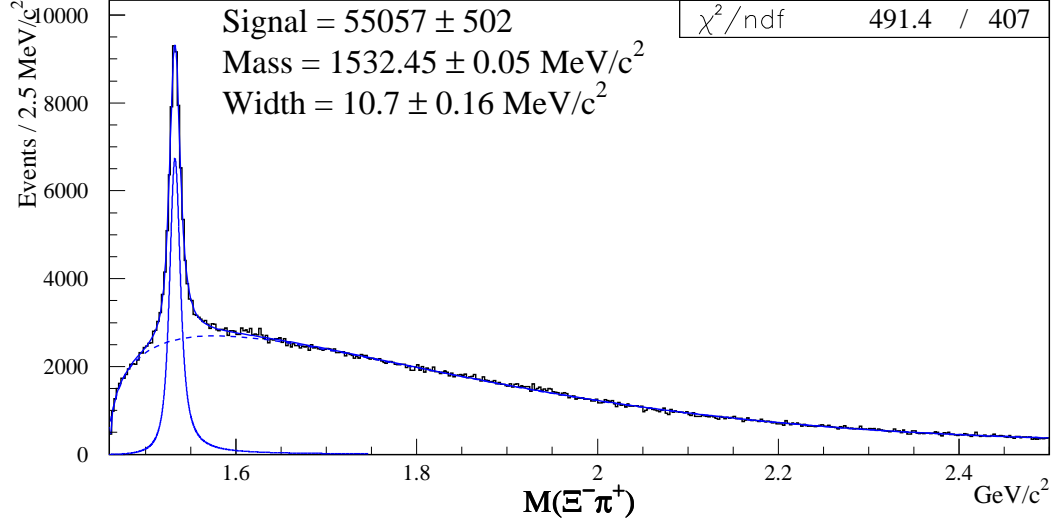


Fig. 4. $\Xi^*(1530)^0$ fit with a P-wave Breit-Wigner for momentum greater than 25 GeV/c and combinatorial background.

jugate states. The combined sample with standard cuts and with an additional momentum cut of 25 GeV/c is plotted in Fig. 6. In this analysis we treat the two samples displayed in Fig. 6 separately, because the production mechanism utilized in Monte Carlo acceptance calculations is much better understood at the higher momenta. The same parameterization of the background is used in Fig. 6 as in Fig. 3 and 4. Such parameterization show acceptable fits to this smooth background as shown in Fig. 7. No evidence for a pentaquark near 1860 MeV/c² or at any mass less than 2400 MeV/c² is observed. To set a limit on the yield we need to make some assumptions about the width of the state. We consider two cases: one with a natural width of 0 and one with a natural width of 15 MeV/c².⁴ In the first case, the signal is fit with a Gaussian with a width given by the experimental resolution. In the second case, the signal is fit with a P-wave Breit-Wigner with an energy dependent width convoluted with the experimental resolution. The experimental resolution σ is parametrized as a function of the invariant mass and we find $\sigma = -9.35 + 7.76m + 0.21m^2$ an adequate approximation, with σ in MeV/c² and m is the mass in GeV/c². With the additional momentum cut of 25 GeV/c the experimental resolution change to $\sigma = -7.99 + 6.29m + 0.62m^2$.

A series of 921 fits to the observed $\Xi^-\pi^-$ mass plot were performed using the background and signal shapes described above for each assumed width. The signal mass is varied in 1 MeV/c steps from 1480 to 2400 MeV/c² and a binned log-likelihood fit using MINUIT [21] is performed. The $\pm 1\sigma$ errors

⁴ NA49 detected this state with a width below the detector resolution of 18 MeV/c². Therefore the expected width of this state cannot exceed this value. A choice of natural width of 15 MeV/c² convoluted with FOCUS resolution in a range of 4-11 MeV/c² gives about 18 MeV/c², the upper limit set by NA49.

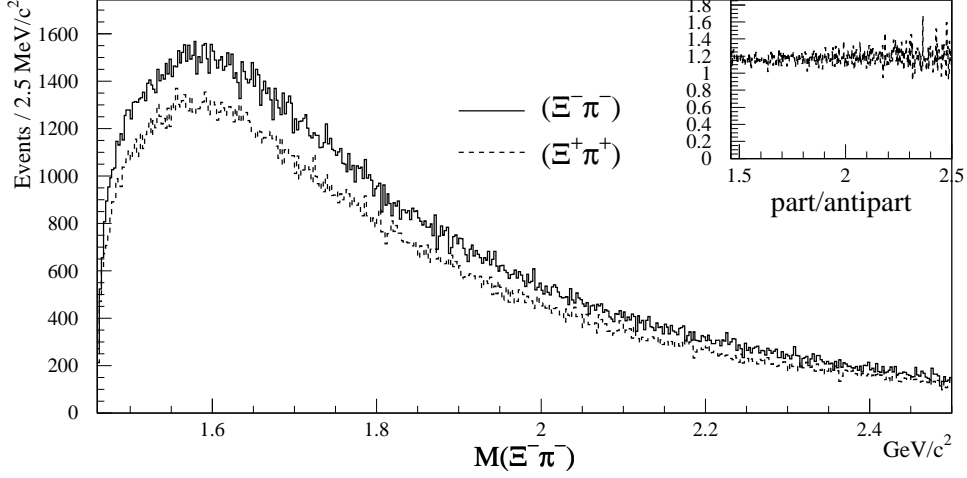


Fig. 5. The invariant mass distribution of $\Xi^- \pi^-$ separated by charge (particle and antiparticle). Standard cuts are applied (no momentum cut). The inset plot is the ratio of particle/antiparticle.

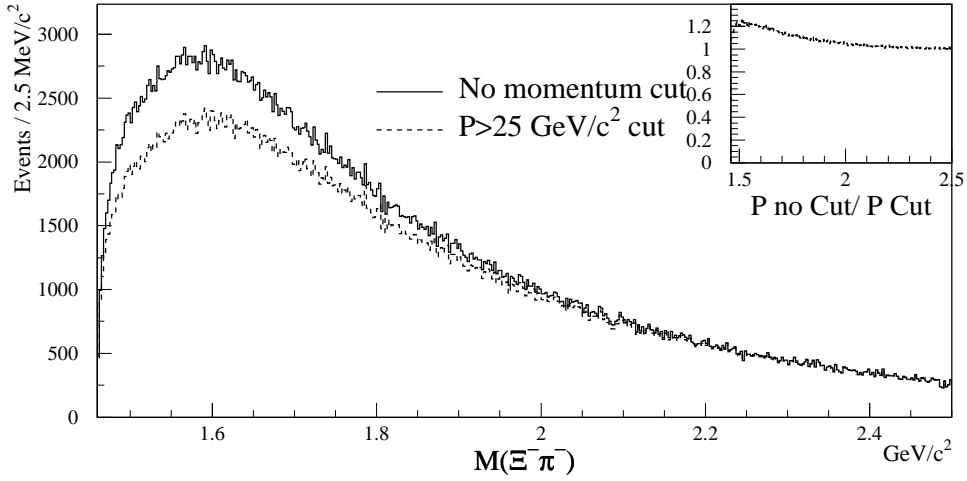


Fig. 6. The invariant mass distribution of $\Xi^- \pi^-$ for particle and antiparticle combined. The solid line shows the result for the standard cuts and the dashed line is with the additional cut that the momentum is greater than 25 GeV/c . The inset plot is the ratio of both, note that the momentum cut affects primarily low mass.

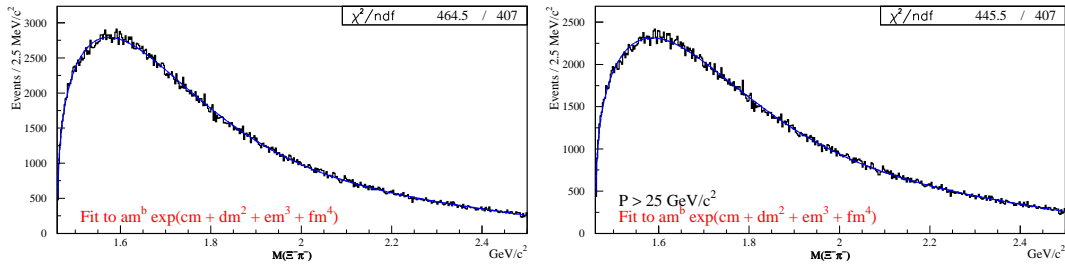


Fig. 7. Fit to the invariant mass distribution of $\Xi^- \pi^-$ for particle and antiparticle combined. The left figure show the result for the standard cuts and the right figure with the additional cut that the momentum is greater than 25 GeV/c .

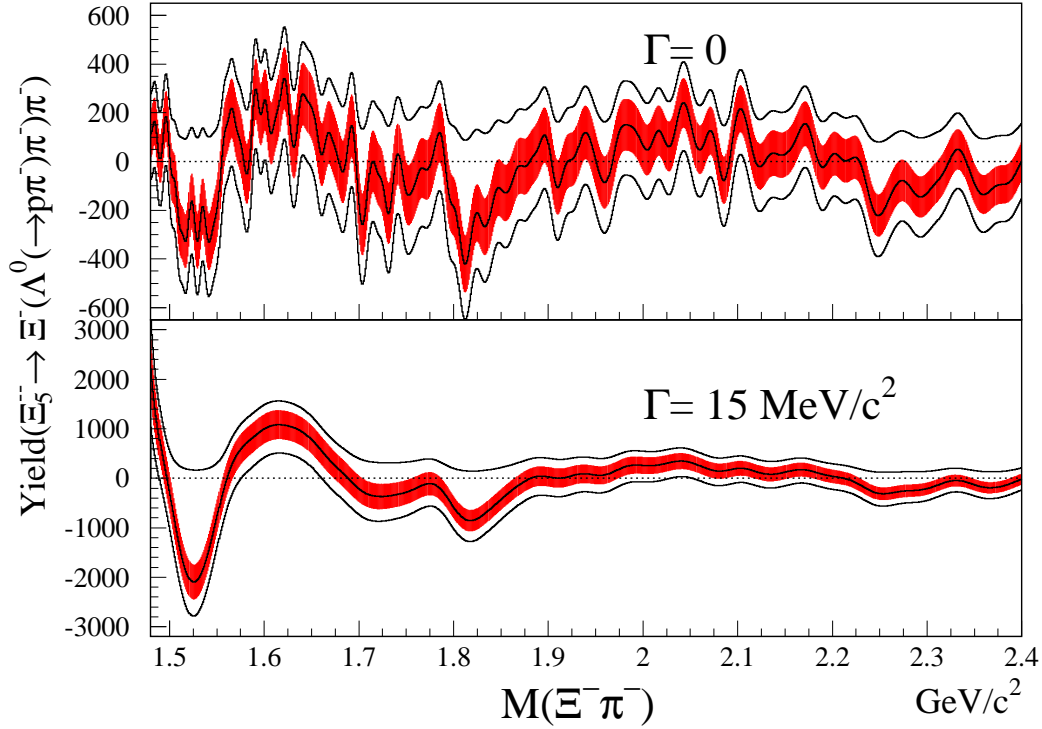


Fig. 8. Pentaquark yields and upper limits. Top (bottom) plots show results for a natural width of 0 ($15 \text{ MeV}/c^2$). The shaded region includes the 1σ errors with the central value in the middle. The outer curves show the upper and lower 95% confidence limits.

are defined as the point where $\Delta \log \mathcal{L} = 0.50$ relative to the maximum $\log \mathcal{L}$, while continually adjusting the background parameters to maximize $\log \mathcal{L}$. The 95% CL lower limit is defined similarly with $\Delta \log \mathcal{L} = 1.92$. Both are obtained using MINOS [21]. The 95% CL upper limit is constructed as follows: The likelihood function \mathcal{L} versus yield is determined by maximizing $\log \mathcal{L}$ for many different (fixed) yields, allowing background parameters to float. The likelihood function is integrated from a yield of 0 to ∞ to obtain the total likelihood. The 95% CL upper limit on the yield is defined as the point where 95% of the total likelihood is between a yield of 0 and the upper limit.⁵ The fitted yield, 1σ errors, and 95% CL limits are shown in Figs. 8 and 9. Of the 1842 fits, none of them finds a positive excursion greater than 5σ . The only previous pentaquark observation was around $1860 \text{ MeV}/c^2$. In this region, we find a small dip which is not statistically significant. The largest positive excursion occurs in the region where the background distribution peaks.

To compare with other experiments, the limits on yield must be converted to limits on production times the (unknown) branching ratio. We choose to

⁵ This definition of an upper limit is used rather than a counting based Feldman–Cousins type limit because errors are Gaussian for this large background.

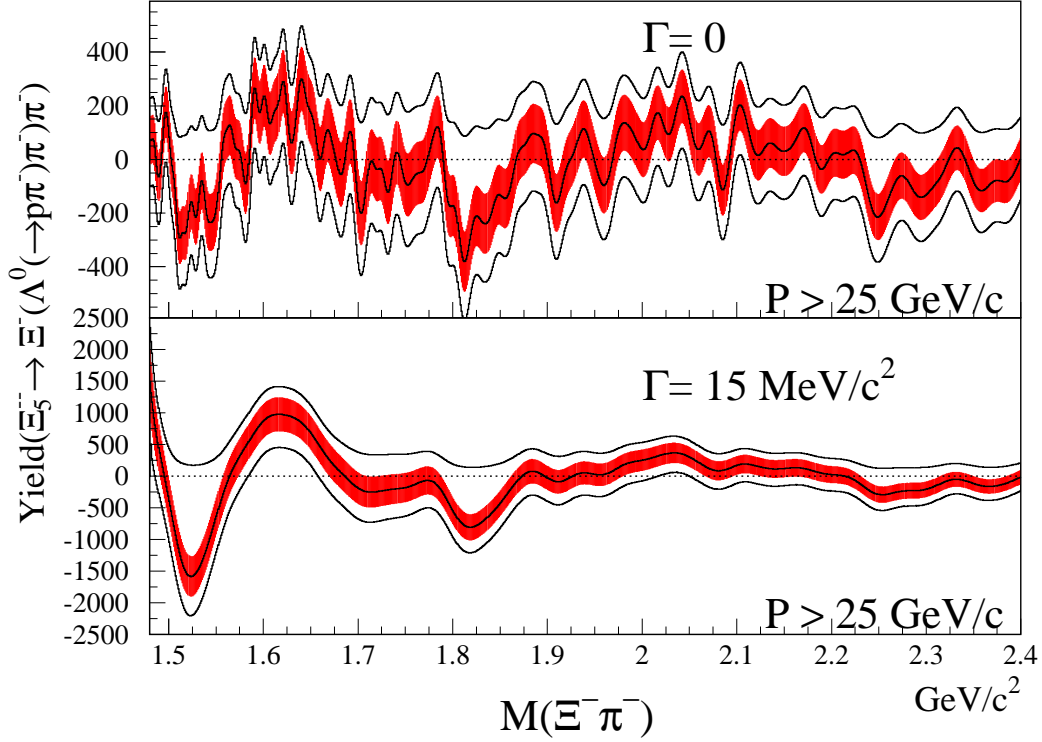


Fig. 9. Pentaquark yield and limits for standard cuts including the 25 GeV/c momentum cut. Top (bottom) plots show results for natural width of 0 (15 MeV/c²). The shaded region includes the 1 σ uncertainty with the central value in the middle. The outer curves show the upper and lower 95% confidence limits.

normalize the Ξ_5^{--} production cross section to $\Xi^*(1530)^0$ because the reconstructed decay mode of the $\Xi^*(1530)^0 \rightarrow \Xi^-\pi^+$ is very similar, in terms of topology and energy release, to the state we are investigating. Thus, we attempt to determine

$$\frac{\sigma(\Xi_5^{--}) \cdot BR(\Xi_5^{--} \rightarrow \Xi^-\pi^-)}{\sigma(\Xi^*(1530)^0)} = \frac{Y(\Xi_5^{--}) \cdot BR(\Xi_5^{--} \rightarrow \Xi^-\pi^-)}{Y(\Xi^*(1530)^0)} \cdot \frac{\epsilon_{\Xi^*(1530)^0}}{\epsilon_{\Xi_5^{--} \rightarrow \Xi^-\pi^-}} \quad (1)$$

All of the efficiencies include the reconstruction and selection efficiencies and corrections for unseen decays of parent particles. The $\Xi^*(1530)^0$ efficiency includes $BR(\Xi^*(1530)^0 \rightarrow \Xi^-\pi^+) = 0.66$ and both efficiencies include the factors $BR(\Xi^- \rightarrow \Lambda^0\pi^-) = 1$ and $BR(\Lambda \rightarrow p\pi^-) = 0.64$. The two branching ratios which are common to both cancel. Determining reconstruction and selection efficiency (including acceptance) is described below.

The FOCUS detector is a forward spectrometer and therefore acceptance depends on the momentum of the produced particle. The production characteristics of the pentaquark are the largest sources of systematic uncertainty in this

analysis. We choose a particular production model to obtain limits and provide sufficient information about the experiment for other interested parties to obtain limits based on other production models. The production simulation begins with a library of e^- and e^+ tracks obtained from a TURTLE simulation [22] of the Wideband beam line. From this library, an individual track is drawn and bremsstrahlung photons are created by passage through a 20% X_0 lead radiator. Photons with energy above 15 GeV are passed to the PYTHIA [23] Monte Carlo simulation. The PYTHIA version we use is 6.127. The PYTHIA simulation is run using minimum bias events⁶ with varying energies.⁷ Options controlling parton distributions and gluon fragmentation were set to avoid heavy quark production.⁸ Since PYTHIA does not produce pentaquarks, another particle must be chosen to represent the pentaquark. According to the string fragmentation model, which is implemented in PYTHIA, the mass of the particle has the greatest effect on production and the number of quarks a particle has in common with the initially interacting hadrons is next in importance. The $\Xi^*(1530)^0$ particle is chosen to represent the production of a pentaquark. The $\Xi^{*0}(ssu)$ can obtain at most 33% of the remaining quarks from the target nucleon valence quarks, while the $\Xi_5^-(ddss\bar{u})$ can take 40%. The charge conjugate $\overline{\Xi^*(1530)^0}(ss\bar{u})$ particles must obtain all quarks from the vacuum, while the $\Xi_5^-(ddssu)$ can take 20% from the target nucleon. The mass of the particle chosen to represent the pentaquark, $\Xi^*(1530)^0$, is set to the appropriate value in PYTHIA.⁹

To calculate the relative cross sections in Eq. 1 we need efficiencies for $\Xi^*(1530)^0 \rightarrow \Xi^-\pi^+$ and $\Xi_5^-- \rightarrow \Xi^-\pi^-$. These efficiencies are obtained from the FOCUS Monte Carlo simulation. The dominant uncertainty in the efficiency determination is the modeling of the production characteristics of the parent particle. For the observed particle, $\Xi^*(1530)^0$, we can compare the data and Monte Carlo directly and adjust the Monte Carlo simulation to produce the correct data distribution. Even this is not sufficient, however, because areas where the efficiency is zero cannot be accounted for. For $\Xi^*(1530)^0$, we run a weighted Monte Carlo simulation which matches the Monte Carlo momentum distribution with the observed data momentum distribution in the region for which the acceptance is not zero. The dominant source of uncertainty for the $\Xi^*(1530)^0 \rightarrow \Xi^-\pi^+$ efficiency is our lack of knowledge of the fraction of events completely outside of our acceptance (momentum less than 15 GeV/c). The weighted PYTHIA Monte Carlo predicts that 71% of the $\Xi^*(1530)^0$ particles are produced with momentum less than 15 GeV/c. To obtain an estimate of the efficiency uncertainty, we assume that the number of particles with mo-

⁶ Specifically MSEL=2 in the PYTHIA setup.

⁷ Specifically MSTP(171)=1 in the PYTHIA setup.

⁸ MSTP(58)=3 to produce light quarks (uds) only and MDME(156--160,1)=0 to limit gluon fragmentation into light quarks only in the PYTHIA setup.

⁹ By setting PMAS(190,1) in PYTHIA.

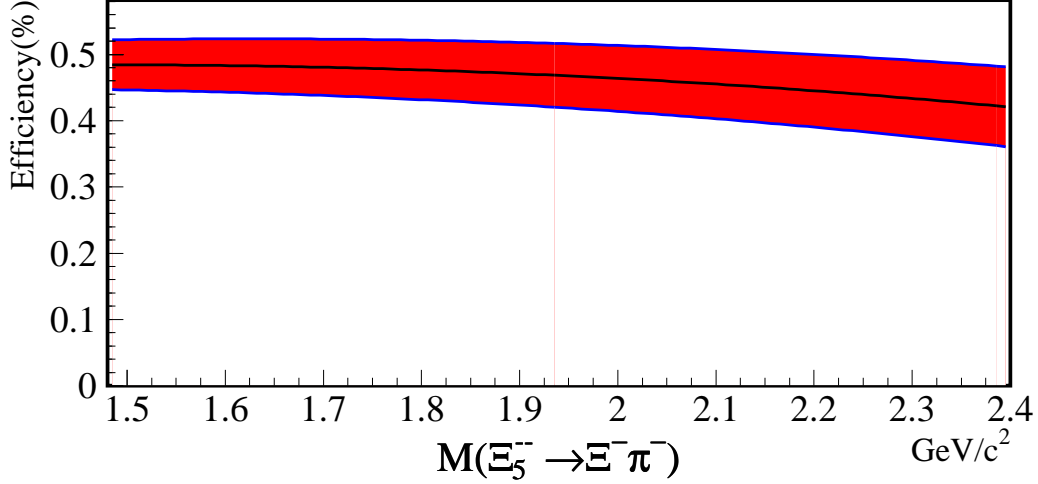


Fig. 10. Acceptance versus mass for pentaquark candidates. Upper (lower) curve is for a 1σ pentaquark produced uncertainty.

momentum less than 15 GeV/ c can be off by as much as a factor of 2 (high or low). This leads to a relative uncertainty on the $\Xi^*(1530)^0$ efficiency of 45%. The $\Xi_5^- \rightarrow \Xi^- \pi^-$ efficiency is taken to match the uncertainty of a higher statistical mode $\Theta^+ \rightarrow p K_S^0$ ($\sim 5\%$) [17] when using a substitute particle like $\Xi^*(1530)^0$ and $\Sigma^*(1385)^+$ to generate pentaquarks with a momenta greater than 25 GeV/ c . The $\Xi_5^- \rightarrow \Xi^- \pi^-$ efficiency versus mass (with no branching ratio corrections) is shown in Fig. 10. The uncertainty in $\epsilon_{\Xi_5^- \rightarrow \Xi^- \pi^-}$ is approximately 10%. The relative uncertainty of the efficiency of an unknown particle ($\sim 10\%$) is indeed less than that for the high statistics normalizing modes ($> 40\%$) because the efficiency uncertainty of the high statistics modes reflects the lack of knowledge of production outside of our acceptance. It is reasonable to assume that discrepancies in the Monte Carlo simulation are similar for the signal mode and the normalizing mode since discrepancies are correlated and therefore adding the uncertainty to the signal mode would be double-counting. Note that the signal and normalizing efficiencies only appear as a ratio.

We also report the relative cross sections in the region where our acceptance is good, that is for parent particle momenta greater than 25 GeV/ c . This dramatically reduces the systematic uncertainties associated with the measurement. The uncertainty due to the production of $\Xi^*(1530)^0$ is minimal. The uncertainty in the Ξ_5^- efficiency is also reduced from approximately 10% to about 5% as shown in Fig. 11. The number of reconstructed $\Xi^*(1530)^0$ at momenta greater than 25 GeV/ c is about 55 000, compared to a total sample of about 65 000 without the momentum cut.

The upper limit on the yield was obtained by mathematically integrating the likelihood function from 0 to infinity and then integrating from 0 to 95% of

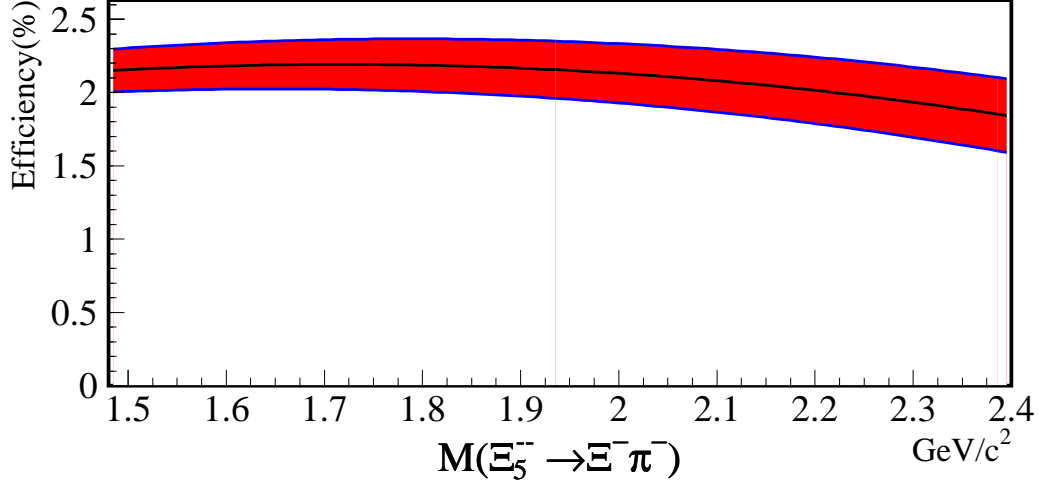


Fig. 11. Acceptance versus mass for pentaquark candidates. Lower (upper) curve is for 1σ pentaquark produced uncertainty. The pentaquark is produced and reconstructed with momentum greater than 25 GeV/c.

the total likelihood integral to obtain the 95% CL upper limit. To obtain the limit on cross section requires a different approach because of the significant systematic uncertainties. We use a method based on a note by Convery [24] which is inspired by the Cousins and Highland [25] philosophy for including systematic uncertainties. The Cousin and Highland prescription is appropriate for low background experiments with Poisson errors while the Convery proposal is applicable to the Gaussian errors which result from the large background in our case. Modifications to the Convery approach are made to give an exact solution [26] when we include efficiency uncertainty systematics.

If systematics are not considered, an analysis using a maximum likelihood fit returns a central value for the branching ratio (\hat{B}) and a statistical error (σ_B). The likelihood function is

$$p(B) \propto \exp \left[\frac{-(B - \hat{B})^2}{2\sigma_B^2} \right]. \quad (2)$$

Including the uncertainty on the efficiency (σ_ϵ) changes the likelihood to:

$$p(B) \propto \frac{1}{\sqrt{\frac{B^2}{\sigma_B^2} + \frac{1}{\sigma_\epsilon^2}}} \exp \left[\frac{-(B - \hat{B})^2}{2(B^2\sigma_\epsilon^2 + \sigma_B^2)} \right] \left\{ \operatorname{erf} \left[\frac{B\hat{B}\sigma_\epsilon^2 + \sigma_B^2}{\sqrt{2}\sigma_\epsilon\sigma_B\sqrt{B^2\sigma_\epsilon^2 + \sigma_B^2}} \right] - \operatorname{erf} \left[\frac{(\hat{S} - 1)\sigma_B^2 - B\sigma_\epsilon^2(B - \hat{B}\hat{S})}{\sqrt{2}\hat{S}\sigma_\epsilon\sigma_B\sqrt{B^2\sigma_\epsilon^2 + \sigma_B^2}} \right] \right\}. \quad (3)$$

We integrate Eq. 3 from 0 to ∞ to obtain the total probability and then

integrate from 0 to the point at which 95% of the total probability is included to obtain the 95% CL upper limit. The branching ratio B of Eq. 3 is simply the relative cross section times the unknown pentaquark branching ratio as in Eq. 1. The relative uncertainties on the efficiency for the signal and normalizing mode are added in quadrature to become σ_ϵ in Eq. 3. Furthermore, \hat{S} is the relative efficiency between the signal and normalizing modes and σ_B is the statistical uncertainty on the branching ratio due simply to the uncertainty in the signal yield.

Figure 12 shows the results for $\frac{\sigma(\Xi_5^{--}) \cdot \text{BR}(\Xi_5^{--} \rightarrow \Xi^- \pi^-)}{\sigma(\Xi^*(1530)^0)}$ with an assumed natural width of 0 (15) MeV/ c^2 for the top (bottom) plot. This is the result corrected for all undetected particles. The shaded band shows the $\pm 1\sigma$ limits with statistical uncertainties only; the line in the middle of the band is the central value. The top curve shows the 95% CL upper limit using the method described above including statistical and systematic uncertainties. The curve between the full upper limit and the 1σ band is the 95% CL upper limit using the method described above with no systematic uncertainties included. The large systematic uncertainties are due to the attempt to correct for the significant fraction of particles outside of our acceptance. While this systematic uncertainty significantly degrades the limit, the production times branching ratio of the pentaquark relative to $\Xi^*(1530)^0$ production is still less than 0.032 (0.091) at 95% CL over the mass range 1.5 to 2.4 GeV/ c^2 for a natural width of 0 (15) MeV/ c^2 . The background, as shown in Figure 7, is rising so rapidly below 1.5 GeV/ c^2 that fitting becomes very sensitive to the form assumed for the background. Consequently we do not quote upper limits below 1.5 GeV/ c^2 .

The plots in Figure 13 show the same results for the restricted range of momentum greater than 25 GeV/ c . That is, they show limits on relative cross sections for particles (Ξ_5^{--} , $\Xi^*(1530)^0$) produced with $p > 25$ GeV/ c .

4 Conclusions

We find no evidence for pentaquarks decaying to $\Xi^- \pi^-$ in the mass range of 1480 MeV/ c^2 to 2400 MeV/ c^2 . In contrast, we observe about 65 000 $\Xi^*(1530)^0 \rightarrow \Xi^- \pi^+$ particles which have a very similar topology and energy release. We set 95% CL upper limits on the yield over the entire mass range with a maximum of 600 (3000) events for an assumed natural width of 0 (15) MeV/ c^2 . We also obtain 95% CL upper limits on the cross section for pentaquark production times the branching ratio to $\Xi^- \pi^-$ relative to $\Xi^*(1530)^0 \rightarrow \Xi^- \pi^+$. These limits are determined for two cases. The first case is for parent particles produced at any momenta where we find a maximum upper limit of $\frac{\sigma(\Xi_5^{--}) \cdot \text{BR}(\Xi_5^{--} \rightarrow \Xi^- \pi^-)}{\sigma(\Xi^*(1530)^0)} < 0.032$ (0.091) at 95% CL for a natural width of 0

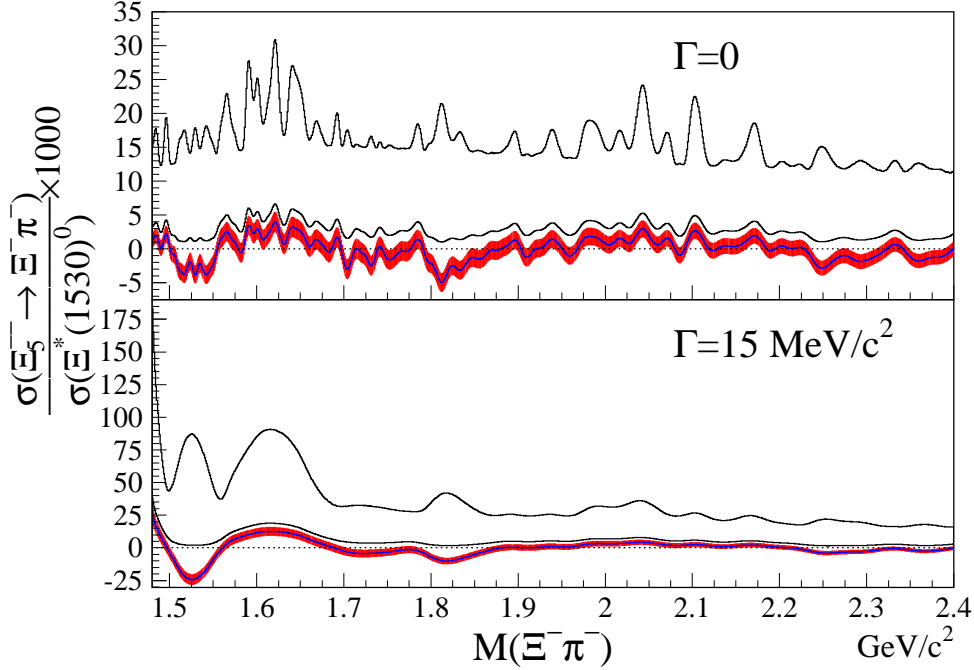


Fig. 12. $\frac{\sigma(\Xi_5^{--}) \times \text{BR}(\Xi_5^{--} \rightarrow \Xi^- \pi^-)}{\sigma(\Xi^*(1530)^0)}$ versus mass. Top (bottom) plots show results for a Ξ_5^{--} natural width of 0 (15 MeV/c²). The shaded region encompasses the 1 σ statistical uncertainty with the central value in the middle. The top curve shows the 95% CL upper limit including systematic uncertainties while the middle curve is the 95% CL upper limit with statistical uncertainties only.

(15) MeV/c². In the second case we measure the relative cross sections for parent particles with momenta above 25 GeV/c (a region of good acceptance) and calculate 95% CL limits of $\frac{\sigma(\Xi_5^{--}) \cdot \text{BR}(\Xi_5^{--} \rightarrow \Xi^- \pi^-)}{\sigma(\Xi^*(1530)^0)} < 0.007$ (0.019) for a natural width of 0 (15) MeV/c².

The only experiment reporting an observation of the Ξ_5^{--} is NA49 [7] which shows about 15 $\Xi^*(1530)^0 \rightarrow \Xi^- \pi^+$ candidates, while reconstructing 38 $\Xi_5^{--} \rightarrow \Xi^- \pi^-$ candidates. The FOCUS results for photon interactions presented here represent samples that are more than 4000 times larger, show no evidence for a state $\Xi_5^{--} \rightarrow \Xi^- \pi^-$, and are in marked contrast with the NA49 results for pp interactions.

5 Acknowledgments

We wish to acknowledge the assistance of the staffs of Fermi National Accelerator Laboratory, the INFN of Italy, and the physics departments of the collaborating institutions. This research was supported in part by the U. S.

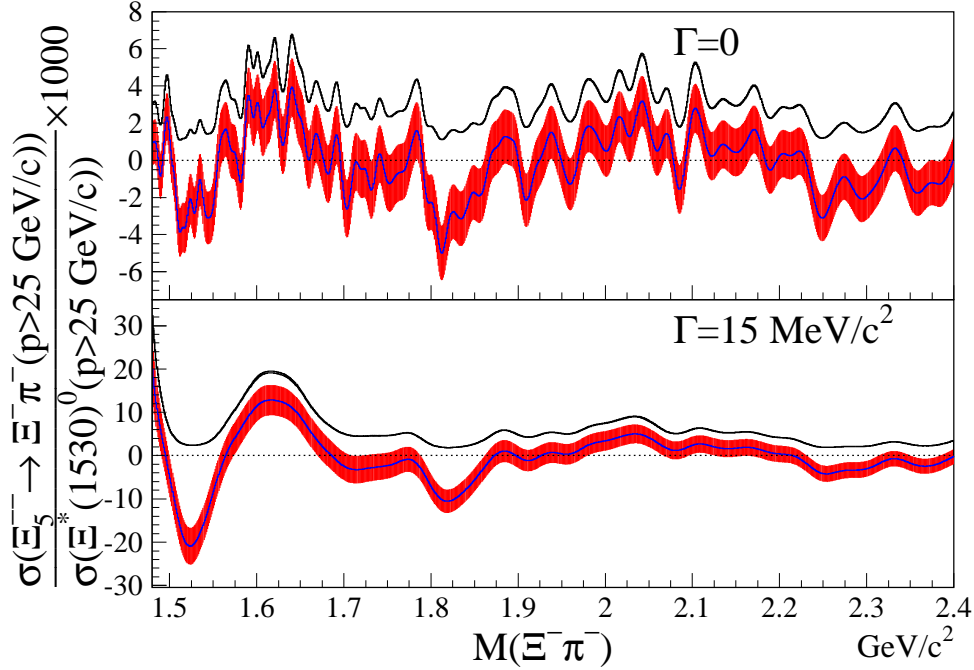


Fig. 13. $\frac{\sigma(\Xi_5^{--}) \times \text{BR}(\Xi^{--} \rightarrow \Xi^- \pi^-)}{\sigma(\Xi^{*}(1530)^0)}$ for $p > 25 \text{ GeV}/c$ versus mass. Top (bottom) plots show results for a Ξ_5^{--} natural width of 0 ($15 \text{ MeV}/c^2$). The shaded region encompasses the 1σ statistical uncertainty with the central value in the middle. The top curve shows the 95% CL upper limit including systematic uncertainties and is virtually indistinguishable from the middle curve which shows the 95% CL upper limit with statistical uncertainties only.

National Science Foundation, the U. S. Department of Energy, the Italian Istituto Nazionale di Fisica Nucleare and Ministero dell'Istruzione dell'Università e della Ricerca, the Brazilian Conselho Nacional de Desenvolvimento Científico e Tecnológico, CONACyT-México, the Korean Ministry of Education, and the Korean Science and Engineering Foundation.

References

- [1] R.L. Jaffe, Phys. Rev. D15 (1977) 267.
- [2] R.L. Jaffe, Phys. Rev. D15 (1977) 281.
- [3] R.L. Jaffe, Phys. Rev. Lett. 38 (1977) 195.
- [4] D. Diakonov, V. Petrov and M.V. Polyakov, Z. Phys. A359 (1997) 305.
- [5] S. Eidelman et al. (Particle Data Group Collaboration), Phys. Lett. B592 (2004) 1.
- [6] R.A. Schumacher, AIP Conf. Proc. 842 (2006) 409.

- [7] C. Alt et al. (NA49 Collaboration), Phys. Rev. Lett. 92 (2004) 042003.
- [8] I. Abt et al. (HERA-B Collaboration), Phys. Rev. Lett. 93 (2004) 212003.
- [9] S. Schael et al. (ALEPH Collaboration), Phys. Lett. B599 (2004) 1.
- [10] M.I. Adamovich et al. (WA89 Collaboration), Phys. Rev. C70 (2004) 022201.
- [11] A. Airapetian et al. (HERMES Collaboration), Phys. Rev. D71 (2005) 032004.
- [12] B. Aubert et al. (BABAR Collaboration), Phys. Rev. Lett. 95 (2005) 042002.
- [13] S. Chekanov et al. (ZEUS Collaboration), Phys. Lett. B610 (2005) 212.
- [14] E.S. Ageev et al. (COMPASS Collaboration), Eur. Phys. J. C41 (2005) 469.
- [15] D.C. Christian et al. (E690 Collaboration), Phys. Rev. Lett. 95 (2005) 152001.
- [16] D.O. Litvintsev (CDF Collaboration), Nucl. Phys. Proc. Suppl. 142 (2005) 374.
- [17] J.M. Link et al. (FOCUS Collaboration), Phys. Lett. B639 (2006) 604.
- [18] J.M. Link et al. (FOCUS Collaboration), Nucl. Instrum. Meth. A516 (2004) 364.
- [19] J.M. Link et al. (FOCUS Collaboration), Nucl. Instrum. Meth. A484 (2002) 174.
- [20] J.M. Link et al. (FOCUS Collaboration), Nucl. Instrum. Meth. A484 (2002) 270.
- [21] F. James et al. (CN/ASD Group Collaboration), CERN (1994).
- [22] D.C. Carey et al. (CN/ASD Group Collaboration), SLAC-R-246,FERMILAB-PM-31 (1982).
- [23] T. Sjöstrand, Comput. Phys. Commun. 82 (1994) 74.
- [24] M.R. Convery, SLAC-TN-03-001.
- [25] R.D. Cousins and V.L. Highland, Nucl. Instrum. Meth. A320 (1992) 331.
- [26] K. Stenson, arXiv.org physics/0605236 (2006).